Hindawi
Advances in Civil Engineering
Volume 2019, Article ID 7069757, 11 pages
https://doi.org/10.1155/2019/7069757

*Research Article*

# Effects of Water Immersion on the Adhesion between Adhesive Layer and Concrete Block

**Jiajun Shi, Yunfeng Pan, Hedong Li, and Jun Fu**

*School of Civil Engineering and Architecture, Zhejiang Sci-Tech University, Hangzhou, China*

Correspondence should be addressed to Yunfeng Pan; yf.poon@foxmail.com

Received 17 July 2019; Revised 11 September 2019; Accepted 30 September 2019; Published 30 October 2019

Academic Editor: Chiara Bedon



The effectiveness of load transfer in the CFRP-adhesive-concrete system highly relies on the integrity of the interfacial bond between adhesive layer and concrete. In the present paper, the effects of water immersion on the mode I fracture energy of the adhesion between CFRP adhesive and concrete were investigated experimentally and numerically. Four-point bending test was conducted to measure the mode I fracture energy of the interfacial layer between adhesive and concrete. The moisture content distribution and the hygrothermal stress were determined by using the finite element method (FEM). The mode I fracture energy was found decreasing with increasing immersion time. The difference between the mode I fracture energy at 2 weeks and 4 weeks is rare. The failure mode of the four-point bending test specimen shifts from concrete failure to interfacial debonding. The moisture content at the adhesive/concrete interface reaches equilibrium after 2 weeks of water immersion. The hygrothermal stress between adhesive and concrete is smaller than the tensile strength of concrete. Deterioration of the physical bond leads to the degradation of bonding strength. The reduction of the mode I fracture energy is more severe than that of the mode II fracture energy.

## 1. Introduction

Strengthening structural members with a carbon fibre-reinforced polymer (CFRP) sheet or plate is becoming more and more popular [1–3]. Debonding failure caused by formation and propagation of the flexural-shear crack at the interface between adhesive and concrete is a common failure mode for the CFRP-adhesive-concrete system. The local stress at the crack tip is composed of a peeling stress (Mode I) and a shear stress (Mode II), as shown in Figure 1. The effectiveness of strengthening with CFRP highly relies on the integrity of the interfacial layer between CFRP adhesive and concrete [2], which may degrade under humid conditions and hygrothermal conditions [4–9]. Lots of studies have investigated the durability of the interfacial layer, in terms of the shear bond stress (Mode II), experimentally [5] and numerically [10]. However, the durability of the interfacial layer in terms of the mode I fracture energy was rarely investigated. The degradation mechanism of the adhesive-concrete interfacial layer needs to be further studied.

Durability of the CFRP-adhesive-concrete system is affected by the performance of concrete, adhesive, CFRP, and the interfacial layers between them [4, 11, 12]. Compared with concrete, the performance of the adhesive and the interfacial layer between adhesive and concrete is more easily affected by water [4, 5, 13]. It was reported that the compressive strength of concrete varies slightly after immersion in water for 2 years [4]. However, after immersion in water for 1 year, 17% reduction was found for the tensile strength of adhesive [14]; for the interfacial layer between concrete and adhesive, its mode I fracture energy was reported to be reduced by 60% after exposure to water for only 2 weeks [5]. Previous publications also reported that the degradation of the interfacial layer caused by different conditioning conditions is different [15, 16].

The performance of the interfacial bonding between the adhesive layer and concrete depends on the strength of physical and interlocking bonding [15]. The water molecules deteriorate the mode I fracture energy of the interfacial layer, as a result of the degradation of the physical bonding, i.e., disruption of the hydrogen bond and the van der Waals force [13, 16–18]. The water molecules at the interfacial zone are mainly from the concrete substrate [19].

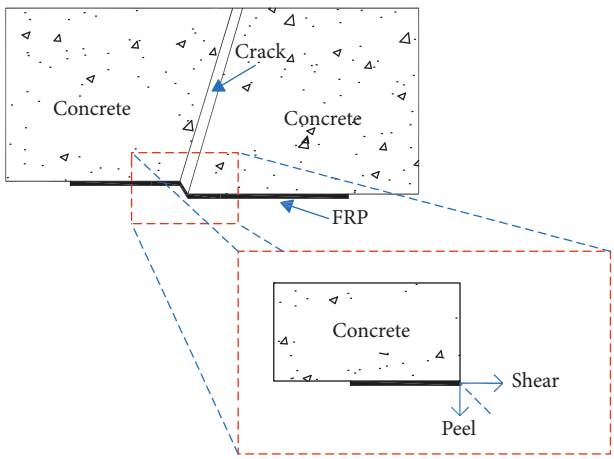


Figure 1: Peeling and shear stress in actual debonding configuration.

Water immersion changes the failure mode of the CFRP-to-concrete system from thin concrete failure to debonding at the interface between adhesive layer and concrete [5]. Under dry condition, the failure usually occurs in concrete beneath the adhesive. But, under wet condition, the adhesive-concrete interfacial debonding always occurs owing to the moisture presence at the interface. This is because the adhesive layer-concrete interfacial bond generally deteriorates more seriously than concrete with moisture presence.

Previous studies showed that the deterioration of the CFRP-adhesive-concrete system depends on the adhesive layer-concrete bond [5, 20]. To evaluate the peel performance, a mixed-mode test was proposed [21]. A movable bottom portion was adopted to control the peel effects on the bond performance. A modified double cantilever beam (MDCB) is a single shear lap-like test setup [5]. The load was applied perpendicular to the FRP. The failure of the bond between FRP and concrete dominates by the combination of peel and shear. The direct tensile test was proposed to evaluate the peel FRP-concrete bonded joint performance under direct tension [22, 23]. The interfacial bond of the strength-based approach is evaluated by the tensile strength. Interfacial fracture energy is a better indicator of the extent of bond degradation than that of the strength-based approach [24]. The effects of material stiffness and sample dimensions are excluded. A four-point bending specimen with sandwiched epoxy layer was chosen to study the Model I of the adhesive layer-concrete bond [25]. The determination of the mode I fracture energy in the sandwiched specimens has been widely carried out [26]. In the present study, the four-point bending specimens were adopted to investigate the involvement of the properties of the adhesive layer-concrete bonded joints.

Previous studies reported that the integrity of the CFRP strengthening concrete structure depends on the bond between the adhesive layer and concrete block in water [5, 15, 25]. Thus, adhesive layer-concrete bonded joints were chosen to evaluate the property evolution of the CFRP strengthening concrete structure. The major objective of the present study was to investigate the effects of water immersion on the peel behavior of the adhesive layer-concrete interfacial layer. The heat transfer module and static analysis module of ABAQUS were, respectively, adopted to determine the moisture distribution and hygrothermal stress at the adhesive layer-concrete interfacial zone. The present paper was expected to shed light on the effects of water molecules on the mechanisms of the adhesive layer-concrete bonded joint at the interface region involved by the physical and interlocking bonds.

## 2. Experimental

*2.1. Raw Materials.* The primer and adhesive used in the present study were provided by Dagong Composite Corp. The properties of the adhesive were determined with so-called dog-bone-shaped samples according to ASTM D638 [27]. The elastic modulus, tensile strength, and ultimate strain of the adhesive were measured to be 3.2 GPa, 57.1 MPa, and 1.9%, respectively. The glass transition temperature ($T_g$) of the adhesive was measured with DMA (three-point bending mode), and $T_g$ was set as the peak of tan delta [28]. $T_g$ of the adhesive was measured to be 80.0°C. The primer was made of the same epoxy with the adhesive.

The weight proportion of the concrete employed was 1.00 : 1.29 : 2.75 : 0.52 (cement: sand : gravel : water). The maximum size of the gravel used is approximately 5 mm. Prepared concrete blocks (40 mm × 40 mm × 40 mm cubes for compressive strength measurement and 40 mm × 40 mm × 160 mm prisms for the bending test) were cured at 95% relative humidity (RH) for one month. The compressive strength of concrete was measured to be 31.8 MPa.

*2.2. Four-Point Bending Test.* Figure 2 shows the schematic sketch of the sandwiched four-point bending test specimen. In order to prepare the specimen, 40 mm × 40 mm × 160 mm concrete prisms were cut into halves along their depth. The cut surface was cleaned with acetone. Low viscosity epoxy primer was then brushed onto the cleaned cut surface, with the pores in the concrete surface filled. The adhesive was brushed onto a rectangular area of 40 mm × 25 mm. The steel strips with 1-mm-thickness were placed between concrete blocks to accurately control the thickness of the adhesive layer. Subsequently, the two concrete blocks of 40 mm × 40 mm × 80 mm size were attached to each other along the longitudinal direction of the concrete blocks. The sandwiched four-point bending specimens were stored for one month in laboratory.

The four-point bending test setup is depicted in Figure 2, in which $l$ is 160 mm. Both $b$ and $d$ are 40 mm. The test was conducted under displacement control as a rate of 0.1 mm/min [29].

*2.3. Exposure Conditions and Absorption of the Adhesive.* The adhesive samples were immersed in water at 20°C. The adhesive specimens of water immersion are 25 mm × 25 mm × 3 mm. The water uptake of the adhesive was weighted periodically. The sample was taken from the

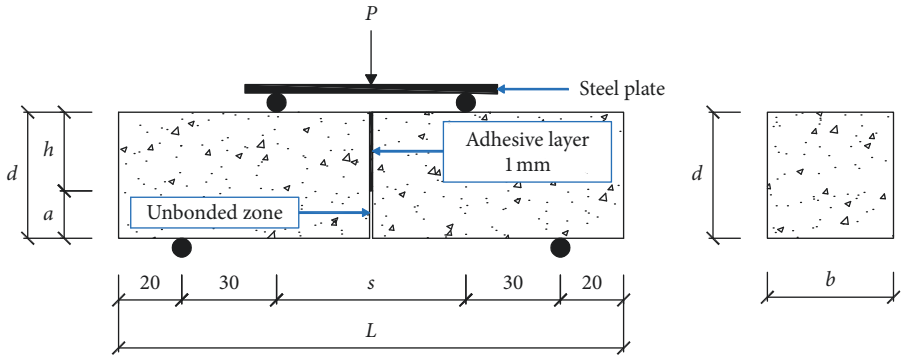


Figure 2: Schematic sketch of the sandwiched four-point bending specimen (all units in mm).

immersion at interval, following by drying the sample surfaces by using a tissue paper. The mass of the samples was weighted by an electronic balance with an accuracy of ±0.01 mg. The exposure conditions of the sandwiched four-point bending specimens were similar to those of the adhesive. The samples were taken out and tested at weekly intervals of 0, 2, and 4.

*2.4. Finite Element Model.* The moisture distribution in the adhesive layer-concrete bonded zone is unavailable to measure. Therefore, the finite element method (FEM) was applied to model the moisture diffusion in the sandwiched four-point bending specimens [30, 31].

Figure 3 shows the 3-dimensional geometrical model of the sandwiched four-point bending specimen. The element type of DC3D8 was used for the transient moisture diffusion. The element size for the concrete block and adhesive layer were 1 mm and 0.1 mm, respectively. To simulate the specimens in water, 100% moisture concentration was specified on the outer surface of the sandwiched four-point bending specimen.

The commercial software ABAQUS is widely used for the transient moisture diffusion. However, the results of the moisture diffusion by the mass diffusion module in ABAQUS are difficult to set as the initial filed for the next step of static analysis. Data transfer from the moisture diffusion to static analysis was achieved by the heat transfer module. Fick's law for mass diffusion is analogous to Fourier's law for heat transfer. The analogy is established as follows:

The normalized concentration analogy can be expressed as [31]

$$\text{temperature } (T) = \text{normalized concentration } (\Phi),$$
$$k = DS, \qquad (1)$$
$$\rho C_p = S,$$

where $T$ is the temperature, $D$ is the moisture diffusivity, $k$ is the thermal conductivity, $C_p$ is the specific heat, and $\phi$ is referred to as the "activity" of the diffusing material and defined as

$$\phi = \frac{C}{S}. \qquad (2)$$

The result of the moisture distribution is set as the boundary conditions of specimens for static analysis. The thermal-hygro analogy is developed as

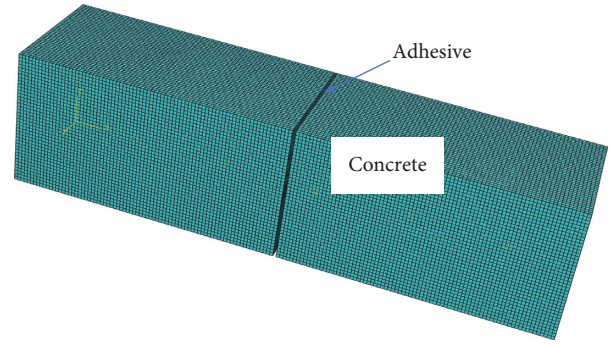


Figure 3: 3-dimensional geometrical model of the sandwiched four-point bending specimen.

$$\alpha = \beta \cdot S, \qquad (3)$$

where $\alpha$ is the thermal expansion coefficient and $\beta$ is the hygroscopic expansion coefficient. Table 1 shows the material properties used in the simulations.

## 3. Results and Discussion

*3.1. Water Absorption by the Adhesive.* The water uptake can be expressed as a function of the square root of the time. The incremental mass of the adhesive proportionally increases with the square root of immersion in Figure 4, following by reaching the equilibrium moisture uptake. Fick's law is extensively adopted to model process of the moisture diffusion [28]. The experimental results are fitted by the simplified Fick's law equation. The simplified form is given as follows:

$$M_t = M_\infty \left\{ 1 - \exp\left[ -7.3 \left( \frac{Dt}{h_a^2} \right)^{0.75} \right] \right\}, \qquad (4)$$

where $M_t$ is the moisture uptake at time $t$, $M_\infty$ is the equilibrium moisture uptake, which is equal to $S$. $D$ is the diffusivity coefficient, and $h_a$ is the thickness of the weighted sample (3 mm for present adhesive specimens). $D$ and $M_\infty$ are obtained by the fitting with equation (4). $D$ and $M_\infty$ are determined to be $63 \times 10^{-9}$ mm$^2$/s and 3.08% (wt.%), respectively. Compared to $D = 78 \times 10^{-9}$ mm$^2$/s and $M_\infty = 2.52\%$ (wt.%) from the reference [17], $D$ decreases by

Table 1: Material properties used in the simulations.

| Materials | Diffusivity coefficient ($mm^2/s$) | Equilibrium moisture content (%) | Hygroscopic expansion coefficient ($H_2O\%$)[a] |
|---|---|---|---|
| Adhesive | $63\times10^{-9}$ | 3.08 | $3.24\times10^{-3}$ |
| Concrete | $1.7\times10^{-5}$ | 7.10 | $5\times10^{-3}$ |

[a]The value of the hygroscopic expansion coefficient was referred to Ref. [32].

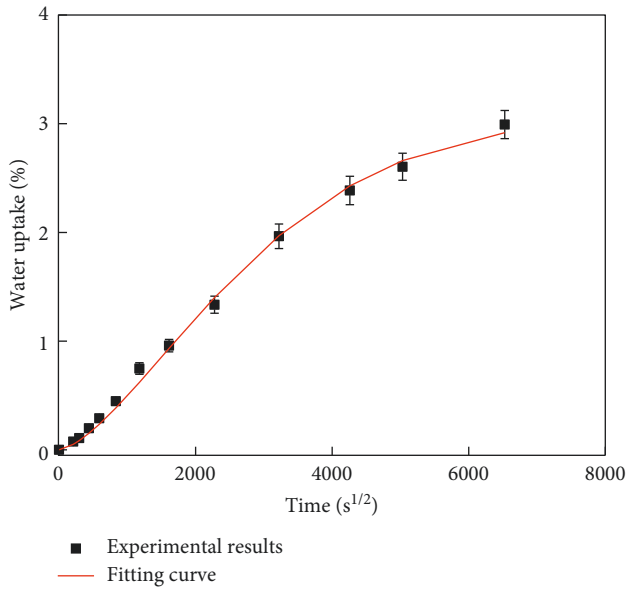


Figure 4: Water uptake curves of the adhesive samples immersed in water.

19%, while $M_\infty$ increases by 17%. It was reported that the extent of the equilibrium moisture content is influenced by the chemical structures of the epoxy system, while does not vary by the environmental temperatures and the immersion duration [33]. The effects of the hydrolysis on the adhesive are significant in water from 300 days to 450 days. The hydrolysis causes a microcrack in the adhesive, and water quickly penetrates into the pores of the adhesive. It results in the larger diffusivity coefficient and equilibrium moisture content.

*3.2. Effects of the Water Uptake on the Properties of the Adhesive.* Figure 5 shows the relationship between the immersion duration and the properties of the adhesive. The water immersion insignificantly influences the properties of the adhesive. The elastic modulus and tensile strength of the adhesive reduce by 1% and 6% after 2 months, respectively. The elongation at break of the adhesive increases with immersion duration from 0 day to 30 days. The elongation at break of the adhesive increases by 29%.

The varied properties of the adhesive depend on the water uptake [14]. The water uptake of the tension specimens differs from the specimens of the water immersion. It results from the size difference of specimens between absorption and the tension of specimens. The longitudinal direction of tension specimens is one order larger than that of the thickness and width. Thus, it is assumed that the water molecules only diffuse along the thickness and width of tension specimens. The tension specimens in thickness and width are 15.0 mm and 3.3 mm, respectively. The relationship between immersion duration and the water uptake can be determined by (4). Figure 6 shows the relationship between the water uptake and the properties of the adhesive. It indicates that the short-term water immersion ($M_\infty < 1.4\%$) insignificantly influences the tensile strength and elastic modulus.

$T_g$ with 2 months of water immersion only decreases by 9%. Water plays the plasticization role in the adhesive within 2 months of water immersion.

*3.3. Failure Modes.* The failure modes of the sandwiched four-point bending specimen are shown in Figure 7. A thin concrete laminate beneath the adhesive was pulled off for the control specimens. The tensile strength of the adhesive and concrete are 57.1 MPa and 1.9 MPa, respectively. The tensile strength of the adhesive is 30 times larger than that of the concrete. The failure modes shifted from a thin concrete failure to adhesive layer-concrete interface separation for the aged specimens. It is attributed to water uptake in the adhesive layer-concrete bonded zone, following the reduction in the bond strength. Compared to the concrete and adhesive laminate, the adhesive layer-concrete bond is the weakest laminate. Thus, the precrack at the unbonded zone cannot kink into the concrete block, and the crack propagates along the adhesive layer-concrete interface.

The sandwiched four-point bending specimen is deformed in four-point (pure) bending. The interface bond is located in the pure bending region. The bond stress between concrete and adhesive only involves the normal stress. The mode I fracture energy is adopted to evaluate the bond performance. The mode I fracture energy of the sandwiched four-point bending specimens can be determined by [25]

$$G = \frac{f_1^2\sigma_r^2\pi a}{\overline{E}_1}, \tag{5}$$

$$f_1 = 1.122 - 1.4\left(\frac{a}{d}\right) + 7.33\left(\frac{a}{d}\right)^2 - 13.08\left(\frac{a}{d}\right)^3 + 14.0\left(\frac{a}{d}\right)^4, \tag{6}$$

$$\sigma_r = \frac{6M}{bd^2}, \tag{7}$$

where $G$ is mode I fracture energy, $f_1$ is a correction factor for four-point pure bending, and $M$ is the moment at the interfacial bond, which is equal to $15P$. $a$, $d$, and $h$ are shown in Figure 1. $a$ is 15 mm, and $h$ is 25 mm.

The mode I interfacial fracture energy of the sandwiched four-point bending specimens was determined by equation (5). Figure 8 shows the relationship between the exposure

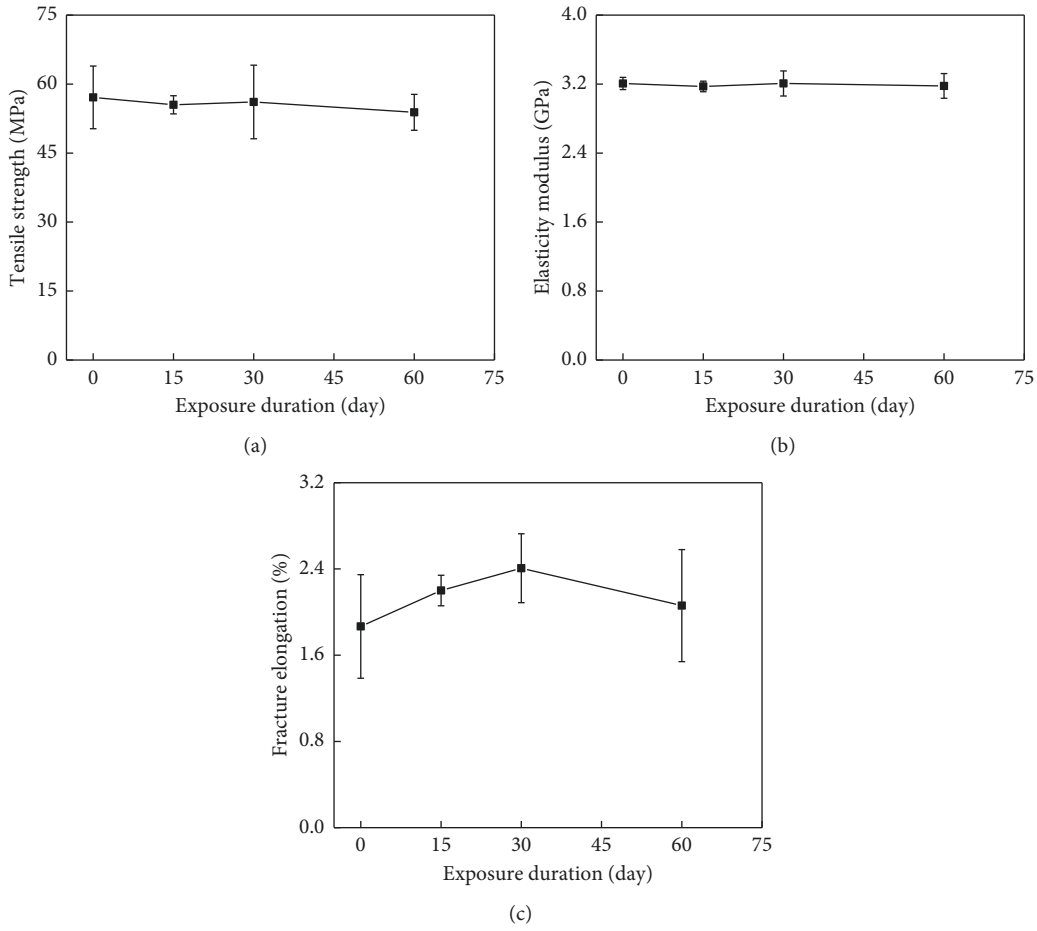


Figure 5: Effects of immersion duration on the tensile strength (a), elastic modulus (b), and fracture elongation (c) of the adhesive.

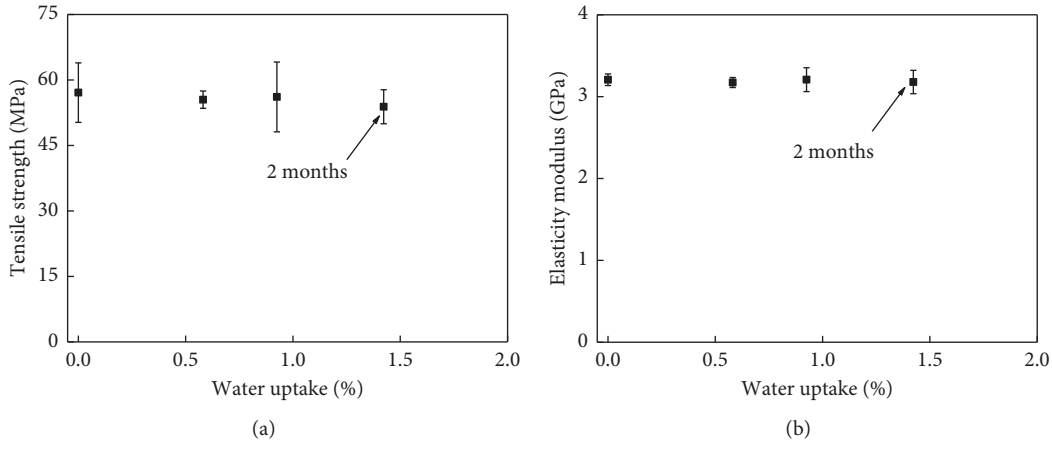


Figure 6: Effects of the water uptake on the tensile strength (a) and elastic modulus (b) of the adhesive.

duration and the mode I fracture energy. The mode I fracture energy reduced by 54% after 2 weeks. The cracking direction can be predicted by [5, 34]

$$\frac{\Gamma_i}{\Gamma_c} \leq 1, \tag{8}$$

where $\Gamma_i$ and $\Gamma_c$ are the interface and concrete fracture energy release rate, respectively. If equation (8) is satisfied, the crack propagates along the interface between adhesive and concrete. The concrete fracture energy was reported to be about 25 J/m$^2$ [5], while the mode I fracture energy of the sandwiched four-point bending specimen reduced to 360 J/m$^2$ and 340 J/m$^2$ after 2 weeks and 4 weeks, respectively. In the case of the sandwiched four-point bending specimen after 2 weeks and 4 weeks, it seems to satisfy equation (8). Thus, the crack should propagate into concrete. In fact,

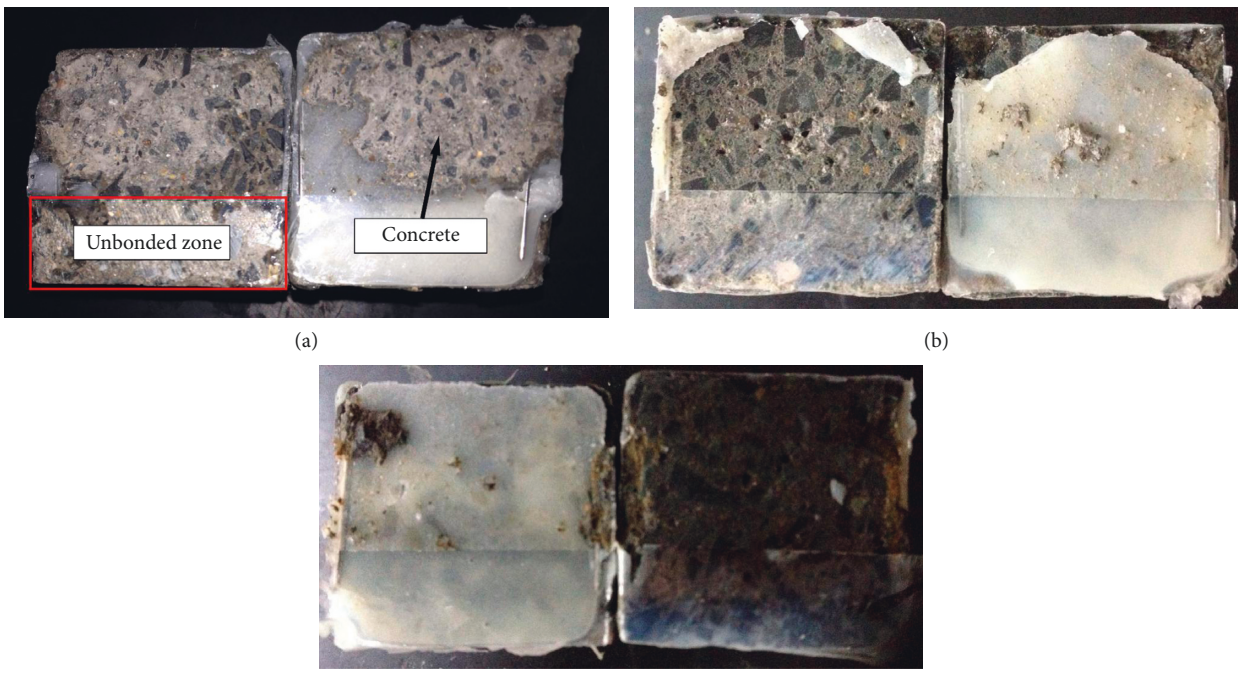


Figure 7: Failure modes of the sandwiched four-point bending specimen: (a) control, (b) after 2 weeks of water immersion, and (c) after 4 weeks of water immersion.

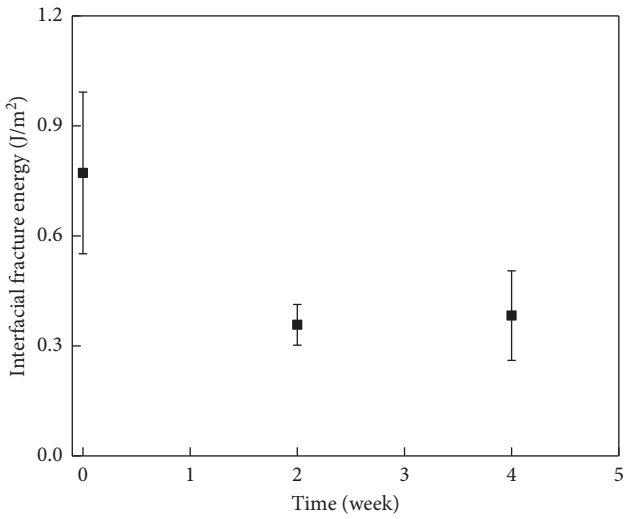


Figure 8: Degradation of the interfacial fracture energy with exposure duration.

Figures 7(b) and 7(c) show the failure mode of the interfacial debonding for specimens in water after 2 weeks and 4 weeks. The crack stayed at the adhesive layer-concrete interface. It means the unsatisfaction of equation (8). It is attributed to the enhancement of the strengthened layer. The strengthened layer involves the penetration of the primer into the pore at the concrete surface. The enhancement results from the fracture energy of the strengthened layer after water immersion, owing to the swelling of the primer. In the case of the aged specimens, the interface fracture energy ($\Gamma_c$) involved in equation (8) is replaced by that of the strengthened layer. Thus, the strengthened layer prevents the crack into concrete.

*3.4. Load-Deformation Behavior of the Sandwiched Four-Point Bending Specimen.* Figure 9 shows the typical load-deformation behavior of the four-point bending for control specimens. It shows that the load linearly increases with the deformation. Less difference of the curve of load-deformation is found for control and aged specimens. All specimens of the ultimate load and corresponding deformation are shown in Table 2. The differences in the load-deformation curves between the aged specimens and control specimens are the ultimate load capacity, initial elastic modulus, and the ultimate deformation. Table 2 shows that the ultimate load capacity and corresponding ultimate deformation rapidly reduce by 31% and 55% after 2 weeks, respectively. The penetration of water uptake at the adhesive-concrete interface causes the degradation of the ultimate load capacity and ultimate deformation. The moisture molecules cause the degradation of the chemical bond and the internal stress, following by the microcrack at the interface. The ultimate load capacity and ultimate deformation insignificantly vary between 2 weeks and 4 weeks of water immersion. It is attributed to the similar failure mode for both specimens exposed to water after 2 weeks and 4 weeks. The initial stiffness ($\alpha$) of the load-deformation behavior is defined in Figure 9. Table 2 shows that the initial stiffness increases with exposure duration. It means that the ductility of the sandwiched four-point bending specimen decreases owing to the water immersion.

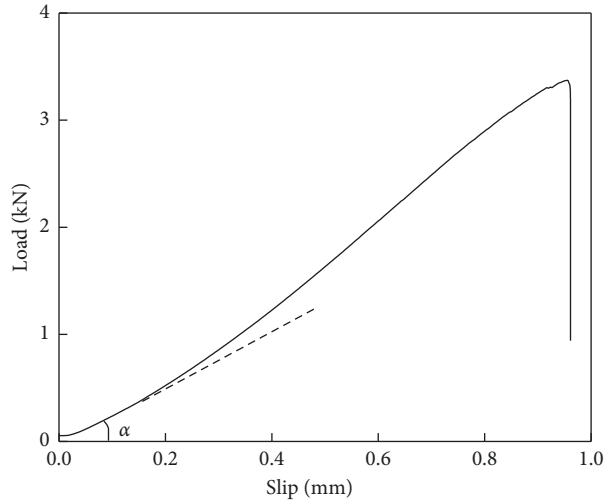


Figure 9: Typical load-deformation behavior of the four-point bending for control specimens.

Table 2: Experimental program and main test result.

| Specimens[a] | Exposure duration (week) | Fracture energy (mJ/mm$^2$) | Ultimate load (kN) | Ultimate slip (mm) | Initial stiffness (N/mm) |
|---|---|---|---|---|---|
| P0W-1 | 0 | 0.46 | 2.27 | 0.57 | 4.1 |
| P0W-2 | 0 | 0.91 | 3.19 | 0.82 | 3.8 |
| P0W-3 | 0 | 0.94 | 3.25 | 0.92 | 3.7 |
| P2W-1 | 2 | 0.37 | 2.04 | 0.37 | 5.3 |
| P2W-2 | 2 | 0.28 | 1.78 | 0.26 | 6.1 |
| P2W-3 | 2 | 0.42 | 2.16 | 0.41 | 3.2 |
| P4W-1 | 4 | 0.50 | 2.38 | 0.28 | 8.0 |
| P4W-2 | 4 | 0.26 | 1.71 | 0.23 | 6.0 |
| P4W-3 | 4 | 0.39 | 2.10 | 0.25 | 7.1 |

[a]0 W, 2 W, and 4 W denote exposure to 0 week, 2 weeks, and 4 weeks of water immersion, respectively. 1, 2, and 3 denote the number of the specimens.

*3.5. Distribution of Moisture Content and Hygroscopic Stress at the Adhesive Layer-Concrete Bonded Zone.* Figure 10 shows typical FEM results in the bond zone of the 3D model of the sandwiched four-point bending specimen. Figure 11 shows the moisture content distribution at the adhesive layer-concrete interface after 2 weeks, 4 weeks, and 6 weeks. Compared to the moisture content close to the center zone, the bond zone on the edge aborts more moisture content. The moisture content on the edge rises simultaneously. The center zone of the water content gradually increases to the water content of the edge zone with the exposure time. The moisture content at the interface mainly migrates from the concrete blocks rather than the adhesive. The diffusivity coefficient of the concrete is two orders of magnitude larger than that of adhesive. The differences in moisture content distribution at the interface do not vary from 2 weeks to 4 weeks. In the case of 2 weeks, most of the moisture content reaches to 2.99%, which is approximately equal to the equilibrium moisture content (e.g., 3.08%).

The water uptake in the adhesive and concrete involves the interfacial internal hygroscopic stress owing to the mismatch of the hygrothermal expansion coefficient between adhesive and concrete. Figure 12 shows the typical FEM results of the hygroscopic stress. In the case of 2 weeks, the hygroscopic stress on the edge is larger than that at the center zone. The shape of the stress distribution is similar to

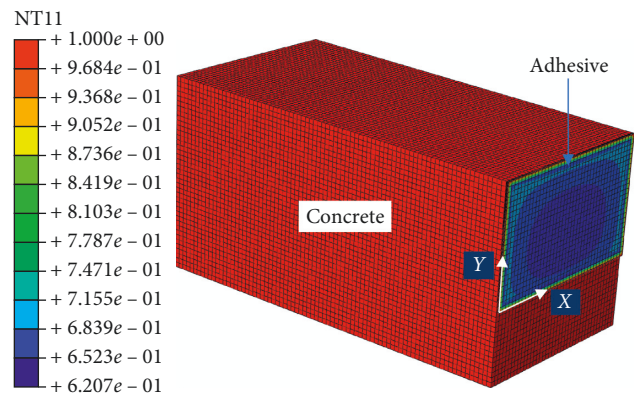


Figure 10: Typical FEM results of moisture content distribution.

that of the moisture content distribution in Figure 11. As discussed, the hygroscopic stress depends on the moisture content. Most of the hygroscopic stress reaches to 1.1 MPa except the interface at the edge. The hygroscopic stress at the edge of the interface is 1.3 MPa. It is attributed to the stress concentration. It is worth noting that the hygroscopic stress is smaller than that of the tensile strength of concrete (1.9 MPa). It means that the there is no microcrack at the interface. It is believed that the reduction in the physical

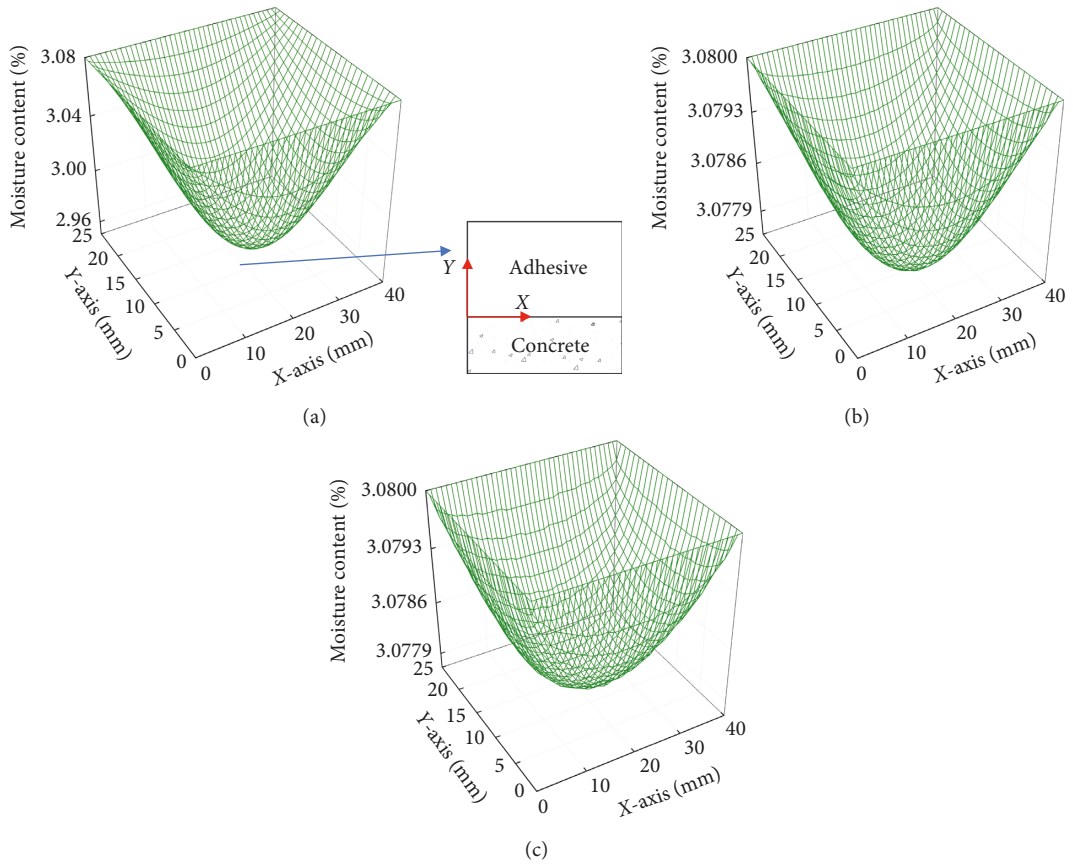


Figure 11: Typical FEM results of the moisture content distribution: (a) 2 weeks, (b) 4 weeks, and (c) 6 weeks.

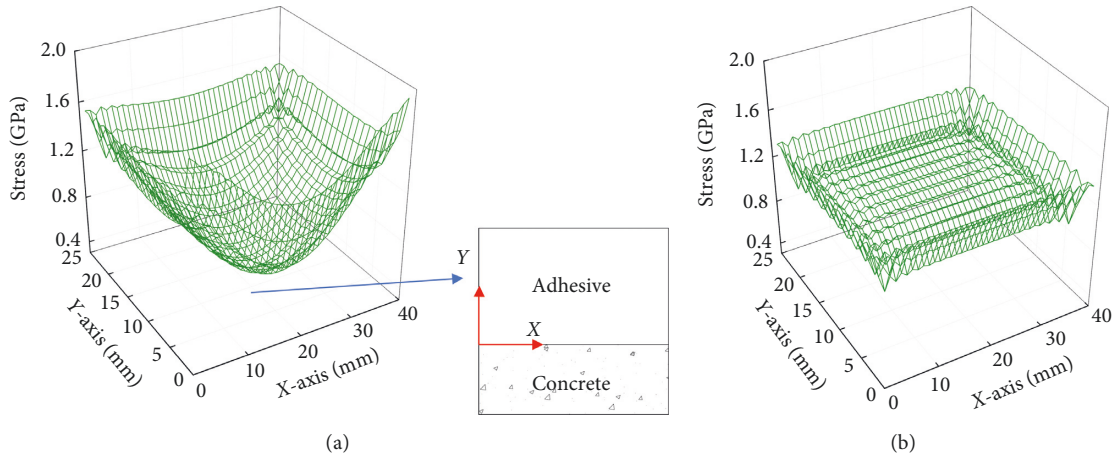


Figure 12: Continued.

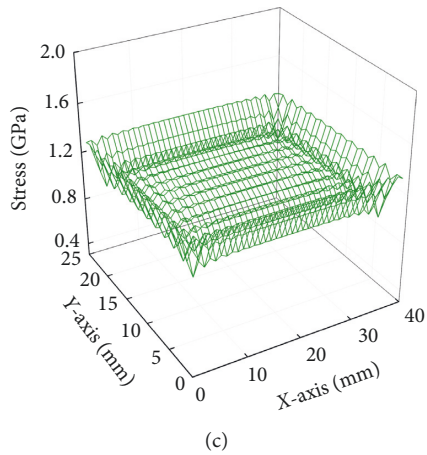


(c)

Figure 12: Typical FEM results of the hygroscopic stress: (a) 2 weeks, (b) 4 weeks, and (c) 6 weeks.

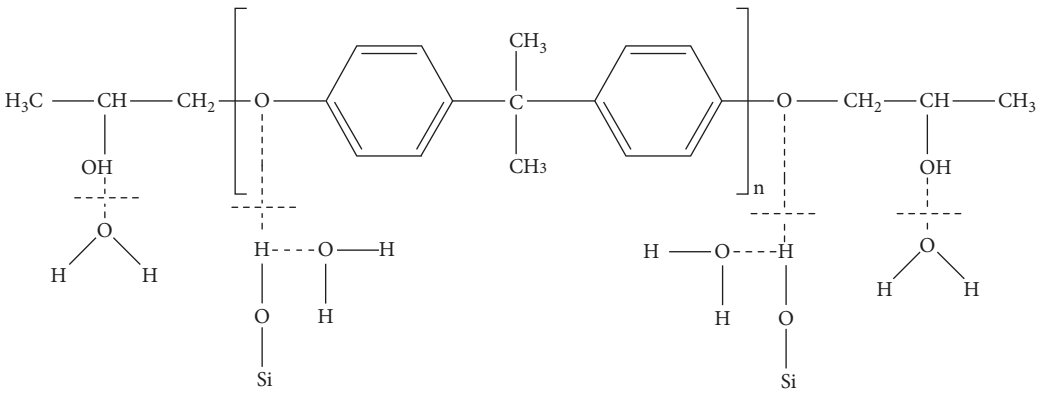

Figure 13: Disruption of the hydrogen bond.

bond mainly causes the degradation of the adhesive layer-concrete bond.

The physical bond is related to the hydrogen bond and the van der Waals force. The water molecules disrupt the hydrogen bond between DGEBA chain (adhesive) and $SiO_2$ (concrete) [17, 35]. In addition, the moisture molecules enlarge the distance between center of mass of the DGEBA chain (epoxy) and $SiO_2$ (concrete). The molecular simulation shows that the binding energy under wet conditions is only one-third of the value attained under dry conditions [35]. Figure 13 shows the disruption of the hydrogen bond.

*3.6. Evolution of Mode I Fracture Energy in Water.* The more literature results [5, 25] are introduced to evaluate the effects of the water immersion on the mode I fracture energy owing to lack of the sufficient long exposure duration in the present study. Figure 14 shows the comparisons of the literature and present results. The water immersion significantly reduces the mode I fracture energy. It is obviously indicated that the normalized fracture energy reduces to be a similar value after four weeks. The residual normalized mode I fracture energy does not vary between four weeks and ten weeks. The degradation in the bond is related to the moisture content at the adhesive layer-concrete interface. The moisture content

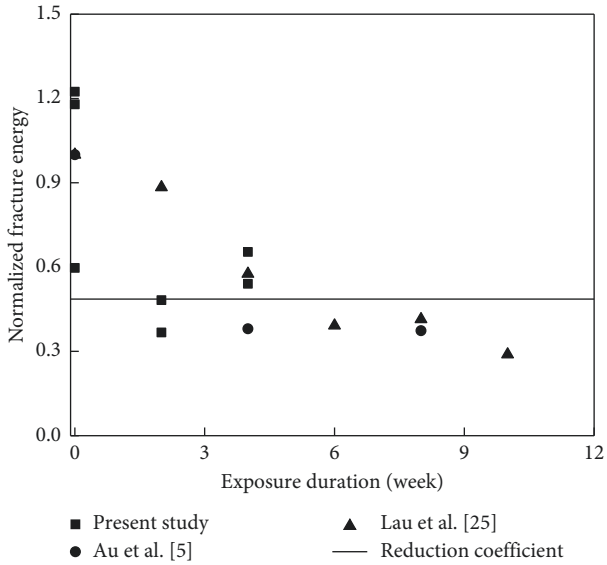


Figure 14: Comparisons of the literature and present results.

reaches a threshold value. Thus, the failure modes shift from concrete cohesive failure to interfacial debonding. The change of the failure mode mainly results in the reduction of the mode I fracture energy. As discussed above, 2 weeks of

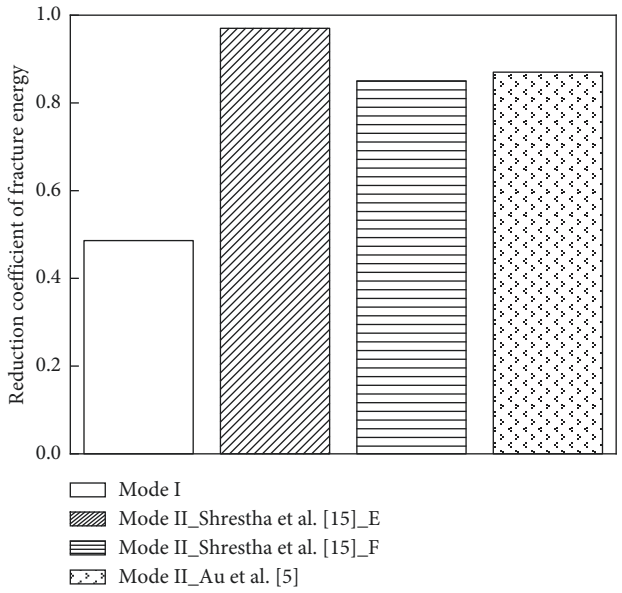


Figure 15: Comparisons of the mode I (peel) fracture energy and mode II (shear) fracture energy.

water immersion in the present study involves an average relative humidity of 98%. The cross section of the concrete block in the present study is similar to that of the literature in Ref. [25]. It is believed that the normalized fracture energy reduced to be a steady value after two weeks. Thus, the average of all the normalized mode I fracture energies after two weeks is 0.486. The reduction coefficient of mode I fracture energy is assumed to be 0.486.

In the application, the deterioration of either mode I fracture energy or mode II fracture energy causes the failure of the FRP strengthening the concrete. The literature results of the evolution of the mode II (shear) fracture energy in water are adopted. It is difficult to directly compare the present samples with the literature samples owing to the differences in the dimension of the samples. As discussed above and in Ref. [5], the degree of the deterioration of the bond performance mainly depends on the water content at the adhesive layer-concrete interface. Thus, the residual mode II fracture energy of the pull-out samples involves the efficient long exposure duration and the similar concrete compressive strength. Figure 15 shows the comparisons of the mode I (peel) fracture energy and mode II (shear) fracture energy. The reduction of the mode I fracture energy is more severe than that of the mode II fracture energy. It means that the mode I fracture energy is more susceptible than mode II fracture energy to the water immersion. The reduction coefficient of the mode I fracture energy is about 50% of that of the mode II fracture energy.

## 4. Conclusions

The major objective of this paper investigated the effect of water immersion on the normal stress using the sandwiched four-point bending specimen experimentally and numerically, and the following conclusions can be drawn:

(1) After 2 weeks of exposure in water, the sandwiched four-point bending specimen is damaged in the separation of the adhesive layer-concrete interface bond. The reduction in ductility and initial stiffness of the sandwiched four-point bending specimen results in the change of the failure mode from concrete cohesive failure to interfacial debonding.

(2) The water molecules significantly reduce the mode I fracture energy. The degradation in the mode I fracture energy involves the moisture content at the adhesive layer-concrete interface.

(3) The evolution of the interfacial bond strength in water seems to be independent of the interlocking bond. The deterioration of the physical bond causes significant reduction of the interface bond strength.

(4) Compared to the reduction in the mode II fracture energy, the mode I fracture energy in water reduces slightly. The residual mode I fracture energy in water reduces to 0.486 of the mode I fracture energy with unaged specimens.

## Data Availability

The data used to support the findings of this study are available from the corresponding author upon request.

## Conflicts of Interest

The authors declare no conflicts of interest.

## Authors' Contributions

Y. P. and H. L. carried out conceptualization. J. F. and Y. P. contributed to methodology. J. S., Y. P. F. J., and Y. Y performed formal analysis and investigation. J. S. and Y. Y wrote the original draft. Y. P. H. L., and J. F. reviewed and edited the manuscript. Y. P was responsible for funding acquisition.

## Acknowledgments

This research was funded by the Zhejiang Provincial Natural Science Foundation of China (Project no. LY19E080029), Production and Construction Group's Programs for Science and Technology Development (Project no. 2019AB016), the Zhejiang Basic Public Welfare Research Project (Project no. LGF8E080016), and the First-Class Disciplines Project of Civil Engineering in Zhejiang Province.

## References

[1] C. Li, G. Xian, and H. Li, "Tension-tension fatigue performance of a large-diameter pultruded carbon/glass hybrid rod," *International Journal of Fatigue*, vol. 120, pp. 141–149, 2019.

[2] J. F. Chen and J. G. Teng, "Anchorage strength models for FRP and steel plates bonded to concrete," *Journal of Structural Engineering*, vol. 127, no. 7, pp. 784–791, 2001.

[3] Y. Wang, X. Li, J. Li, Q. Wang, B. Xu, and J. Deng, "Debonding damage detection of the CFRP-concrete interface based on

piezoelectric ceramics by the wave-based method," *Construction and Building Materials*, vol. 210, pp. 514–524, 2019.

[4] J. Shrestha, D. W. Zhang, and T. Ueda, "Durability performances of carbon fiber–reinforced polymer and concrete-bonded systems under moisture conditions," *Journal of Composites for Construction*, vol. 20, no. 5, Article ID 04016023, 2016.

[5] C. Au and O. Büyüköztürk, "Peel and shear fracture characterization of debonding in FRP plated concrete affected by moisture," *Journal of Composites for Construction*, vol. 10, no. 1, pp. 35–47, 2006.

[6] F. Al-Mahmoud, J.-M. Mechling, and M. Shaban, "Bond strength of different strengthening systems—concrete elements under freeze-thaw cycles and salt water immersion exposure," *Construction and Building Materials*, vol. 70, pp. 399–409, 2014.

[7] H. Liang, S. Li, Y. Lu, and T. Yang, "Reliability analysis of bond behaviour of CFRP-concrete interface under wet-dry cycles," *Materials*, vol. 11, no. 5, p. 741, 2018.

[8] M.-W. Wei, J.-H. Xie, H. Zhang, and J.-L. Li, "Bond-slip behaviors of BFRP-to-concrete interfaces exposed to wet/dry cycles in chloride environment," *Composite Structures*, vol. 219, pp. 185–193, 2019.

[9] J. Li, J. Xie, F. Liu, and Z. Lu, "A critical review and assessment for FRP-concrete bond systems with epoxy resin exposed to chloride environments," *Composite Structures*, vol. 229, p. 111372, 2019.

[10] Y. Tao and J.-F. Chen, "Concrete damage plasticity model for modeling FRP-to-concrete bond behavior," *Journal of Composites for Construction*, vol. 19, no. 1, Article ID 04014026, 2014.

[11] C. Li, G. Xian, and H. Li, "Water absorption and distribution in a pultruded unidirectional carbon/glass hybrid rod under hydraulic pressure and elevated temperatures," *Polymers*, vol. 10, no. 6, p. 627, 2018.

[12] Z. Lu, J. Xie, H. Zhang, and J. Li, "Long-term durability of basalt fiber-reinforced polymer (BFRP) sheets and the epoxy resin matrix under a wet-dry cyclic condition in a chloride-containing environment," *Polymers*, vol. 9, no. 12, p. 652, 2017.

[13] Y. Pan, J. Shi, and G. Xian, "Experimental and numerical study of the CFRP-to-concrete bonded joints after water immersion," *Composite Structures*, vol. 218, pp. 95–106, 2019.

[14] B. Hong and G. Xian, "Ageing of a thermosetting polyurethane and its pultruded carbon fiber plates subjected to seawater immersion," *Construction and Building Materials*, vol. 165, pp. 514–522, 2018.

[15] J. Shrestha, T. Ueda, and D. W. Zhang, "Durability of FRP concrete bonds and its constituent properties under the influence of moisture conditions," *Journal of Materials in Civil Engineering*, vol. 27, no. 2, Article ID A4014009, 2014.

[16] L.-h. Tam and D. Lau, "Moisture effect on the mechanical and interfacial properties of epoxy-bonded material system: an atomistic and experimental investigation," *Polymer*, vol. 57, pp. 132–142, 2015.

[17] Y. Pan, G. Xian, and M. A. G. Silva, "Effects of water immersion on the bond behavior between CFRP plates and concrete substrate," *Construction and Building Materials*, vol. 101, pp. 326–337, 2015.

[18] A. Zhou, O. Büyüköztürk, and D. Lau, "Debonding of concrete-epoxy interface under the coupled effect of moisture and sustained load," *Cement and Concrete Composites*, vol. 80, pp. 287–297, 2017.

[19] Z. Ouyang and B. Wan, "Modeling of moisture diffusion in FRP strengthened concrete specimens," *Journal of Composites for Construction*, vol. 12, no. 4, pp. 425–434, 2008.

[20] S. Amidi and J. Wang, "Subcritical debonding of FRP-to-concrete bonded interface under synergistic effect of load, moisture, and temperature," *Mechanics of Materials*, vol. 92, pp. 80–93, 2016.

[21] J. Pan and C. K. Y. Leung, "Debonding along the FRP-concrete interface under combined pulling/peeling effects," *Engineering Fracture Mechanics*, vol. 74, no. 1-2, pp. 132–150, 2007.

[22] O. R. Mata and R. A. Atadero, "Evaluation of pull-off tests as a FRP-concrete bond testing method in the laboratory and field," *Practice Periodical on Structural Design and Construction*, vol. 19, no. 2, Article ID 04014001, 2014.

[23] ACI, *Guide Test Methods for Fiberreinforced Polymers (FRPs) for Reinforcing or Strengthening Concrete Structures*, Vol. 440, ACI Committee, Farmington Hills, MI, USA, 2012.

[24] J.-G. Dai, H. Yokota, M. Iwanami, and E. Kato, "Experimental investigation of the influence of moisture on the bond behavior of FRP to concrete interfaces," *Journal of Composites for Construction*, vol. 14, no. 6, pp. 834–844, 2010.

[25] D. Lau and O. Büyüköztürk, "Fracture characterization of concrete/epoxy interface affected by moisture," *Mechanics of Materials*, vol. 42, no. 12, pp. 1031–1042, 2010.

[26] Z. Suo and J. W. Hutchinson, "Sandwich test specimens for measuring interface crack toughness," *Materials Science and Engineering: A*, vol. 107, pp. 135–143, 1989.

[27] ASTM, *Standard Test Method for Tensile Properties of Plastics*, ASTM International, West Conshohocken, PA, USA, 2014.

[28] Z. Lu, G. Xian, and H. Li, "Effects of thermal aging on the water uptake behavior of pultruded BFRP plates," *Polymer Degradation and Stability*, vol. 110, pp. 216–224, 2014.

[29] Y. Pan and G. Xian, "Influence of long-term outdoor exposure in a frigid zone on the CFRP-to-concrete bond behavior," *Construction and Building Materials*, vol. 215, pp. 462–474, 2019.

[30] X. Xu, Q. Huang, Y. Ren, D.-Y. Zhao, J. Yang, and D.-Y. Zhang, "Modeling and separation of thermal effects from cable-stayed bridge response," *Journal of Bridge Engineering*, vol. 24, no. 5, Article ID 04019028, 2019.

[31] S. Yoon, B. Han, and Z. Wang, "On moisture diffusion modeling using thermal-moisture analogy," *Journal of Electronic Packaging*, vol. 129, no. 4, pp. 421–426, 2007.

[32] T. K. Tsotsis and Y. Weitsman, "Energy release rates for cracks caused by moisture absorption in graphite/epoxy composites," *Journal of Composite Materials*, vol. 24, no. 5, pp. 483–496, 1990.

[33] G. Xian and V. M. Karbhari, "DMTA based investigation of hygrothermal ageing of an epoxy system used in rehabilitation," *Journal of Applied Polymer Science*, vol. 104, no. 2, pp. 1084–1094, 2007.

[34] M.-Y. He and J. W. Hutchinson, "Kinking of a crack out of an interface," *Journal of Applied Mechanics*, vol. 56, no. 2, pp. 270–278, 1989.

[35] O. Büyüköztürk, M. J. Buehler, D. Lau, and C. Tuakta, "Structural solution using molecular dynamics: fundamentals and a case study of epoxy-silica interface," *International Journal of Solids and Structures*, vol. 48, no. 14-15, pp. 2131–2140, 2011.